

# Full quantum state control of chiral molecules

JuHyeon Lee<sup>1</sup>, Elahe Abdiha<sup>1</sup>, Boris G. Sartakov<sup>1</sup>, Gerard Meijer<sup>1</sup>,  
Sandra Eibenberger-Arias<sup>1\*</sup>

<sup>1</sup>Fritz-Haber-Institut der Max-Planck-Gesellschaft; Berlin, 14195, Germany.

\*Corresponding author. Email: eibenberger@fhi-berlin.mpg.de

**Abstract:** Controlling the internal quantum states of chiral molecules for a selected enantiomer has a wide range of fundamental applications. Using tailored microwave fields, a chosen rotational state can be enriched for a selected enantiomer, even starting from a racemic mixture. This enables rapid switching between samples of different enantiomers in a given state, holding great promise, for instance, for measuring parity violation in chiral molecules. Achieving full enantiomer-specific state transfer is a key requirement for this and many other applications. Although theoretically feasible, achieving the required experimental conditions seemed unrealistic. Here, we realize near-ideal conditions, overcoming both the limitations of thermal population and spatial degeneracy in rotational states. Our results show that 96% state-specific enantiomeric purity can be obtained from a racemic mixture, in an approach that is universally applicable to all chiral molecules of  $C_1$  symmetry.

Homochirality in living organisms, i.e. the preference for one enantiomer, is key to the origins of life, yet the exact mechanism behind it is still unclear. Among the various hypotheses (1-3), it is suggested that parity-violating energy differences between enantiomers, caused by the electro-weak force, can have initiated the chiral imbalance (4). However, despite having been predicted for decades, parity violation in chiral molecules has not yet been experimentally observed (5-7).

Since Pasteur's discovery of optical activity, numerous chiral analysis techniques, such as optical rotation, circular dichroism, and Raman optical activity have been developed (8-11). These traditional methods inherently produce weak signals due to their reliance on weak interactions of the sample with the magnetic field of the light (12). Recently, research on chiral molecules has been rejuvenated by the emergence of new types of spectroscopic methods that rely exclusively on strong electric-dipole interactions. These include Coulomb explosion imaging (13), photo-electron circular dichroism (14, 15), and microwave three-wave mixing (16, 17). These methods are well-suited for studies on dilute samples as they offer remarkably strong enantiomer-sensitive responses.

Enantiomer-specific state transfer (ESST) is a particularly intriguing extension of microwave three-wave mixing. Beyond chiral analysis, ESST enables enantiomer-specific control over the population in rotational states (18, 19). While ESST has thus far experimentally only been demonstrated for rotational states, theoretically, it can be extended to vibrational and electronic degrees of freedom (20, 21). ESST utilizes a unique spectroscopic feature of chiral molecules of  $C_1$  symmetry, i.e., molecules that have no symmetry operation other than the identity. These molecules possess closed triads of electric-dipole-allowed transitions between rotational states (22), which is the key property that enables differentiation between enantiomers. The enantiomer-selectivity of ESST is mathematically governed by the triple product of the three components of the electric dipole moment, that has opposite signs for different enantiomers. In principle, when only a single state is initially populated and when the spatial degeneracy is properly addressed, ESST can reach 100% efficiency.

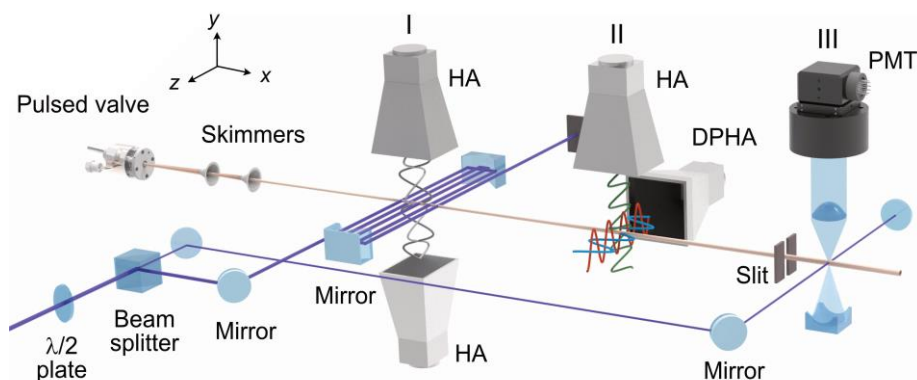


**Fig. 1. Scheme of the experimental setup.** Jet-cooled 1-indanol passes through two skimmers and then traverses three distinct regions (I-III). In (I), the molecules interact with both the UV depletion laser and with MW fields that drive the  $b$ -type transition. The optical multi-pass setup extends the interaction time to  $\sim 30 \mu\text{s}$ . In (II), the molecules interact with a sequence of three orthogonally, linearly polarized MW fields. In (III), the target rotational state is probed using the same UV laser as used for depletion. The laser-induced fluorescence is detected using a photo-multiplier tube (PMT). HA and DPHA denote horn antenna and dual-polarization horn antenna, respectively.

In the ideal scenario, where only one state is populated and there is a single Rabi frequency for each of the three transitions, perfect transfer efficiency can be achieved using a  $\pi/2 - \pi - \pi/2$  pulse sequence (23, 24). In this sequence, the  $\pi/2$  pulses generate maximum coherence between states and the  $\pi$  pulse exchanges population between states. However, early ESST studies reported only modest state-specific enantiomeric enrichment, limited to a few percent (18, 19). This is primarily due to the thermal population of rotational states, which prevails even at rotational temperatures of around 1 K that can be achieved in molecular beams, for instance. In addition, the spatial degeneracy of these states often results in multiple Rabi frequencies for each of the three transitions (24-26). To mitigate the effect of thermal population, ultraviolet (UV) or additional microwave (MW) radiation has been used to deplete one of the rotational states before the ESST process (27-29), thereby significantly enhancing the transfer efficiency. The issue of multiple Rabi frequencies due to spatial degeneracy is circumvented when targeting a triad of rotational states that includes the absolute rotational ground state (30). In this way it has been possible to perform the first quantitative study of ESST (27), albeit under conditions that were not yet ideal.

The present study reports on the experimental realization of the ideal scenario for enantiomer-specific state transfer. By employing MW-UV double resonance in the depletion setup, the thermal population from two rotational states of the triad is removed prior to ESST. Full state-specific enantiomeric enrichment can be obtained by applying this two-level depletion scheme to a triad of rotational states that includes the rotational ground state.

The experimental setup is schematically depicted in Fig. 1. The chiral molecule 1-indanol is heated to  $\sim 80^\circ\text{C}$  and seeded into neon. The gas mixture is expanded at  $\sim 2$  bar backing pressure out of a pulsed valve, operated at 30 Hz, into vacuum. The thus produced jet-cooled molecular beam has a rotational temperature of  $\sim 1$  K and a speed of  $\sim 800$  m/s. The molecular beam is collimated by two skimmers of 3 mm and 1 mm diameter opening, and subsequently passes through the depletion region (I), the ESST region (II), and the detection region (III), as outlined below. The relevant rotational states and MW frequencies of 1-indanol are depicted in Fig. 2A. Details of the excitation schemes at the interaction regions are illustrated in Fig. 2B and 2C. As indicated in these figures, states  $|1_{01}\rangle$  and  $|1_{10}\rangle$  are

depleted in region (I), population is transferred between all three states in region (II), and the population in the target state  $|1_{01}\rangle$  is monitored in region (III).

In the depletion region (I), about 40 mW of tunable continuous-wave UV laser radiation with a bandwidth less than 1 MHz crosses the molecular beam perpendicularly in a multi-pass arrangement. In this way, the total interaction time of the molecules with the UV radiation is extended. The laser frequency is set to selectively excite from the target rotational state  $|1_{01}\rangle$  to the electronically excited state on the  $S_1(2_{02}) \leftarrow S_0(1_{01})$  R-branch line (31), addressing all  $M_J$  sub-levels. Once excited, the molecules rapidly radiate, predominately to higher vibrational states and other rotational states within the  $S_0$  electronic state (32). For the small fraction of molecules that radiates back to the original state, the process is repeated, effectively depleting the  $|1_{01}\rangle$  state. Simultaneously, MW fields that drive the  $b$ -type transition are applied to connect state  $|1_{10}\rangle$  to the target state  $|1_{01}\rangle$ , thereby depleting both levels via optical pumping. The polarization of these MW fields is switched back and forth between the  $\hat{z}$ - and  $\hat{x}$ - directions, thereby coupling all  $M_J$  sub-levels of the rotational states. This is crucial for complete depletion, as otherwise, according to the selection rules, the  $M_z = 0$  sub-level in state  $|1_{10}\rangle$  would remain populated. In Fig. 2B it is shown, how the different  $M_z$  sub-levels are addressed by each MW polarization direction. Further details are given in the Supplementary Materials.

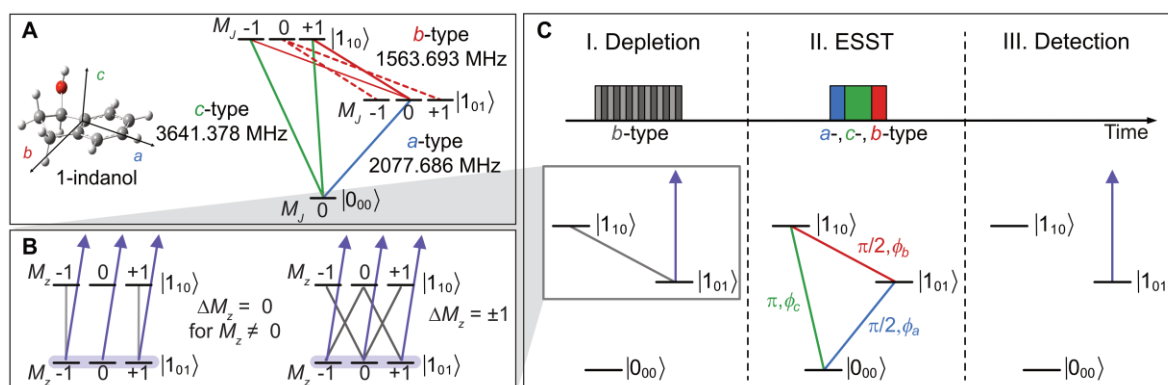


**Fig. 2. Schemes of the experimental procedure using 1-indanol.** (A) Illustration of the triad of rotational states of 1-indanol used in this study, shown in standard spectroscopic notation  $|J_{K_a K_c}\rangle$ . All  $M_J$  sub-levels and allowed transitions are represented, with frequencies and types of MW transitions marked. (B) Depiction of depletion schemes using MW-UV double resonance. Two scenarios are presented: using polarization along  $\hat{z}$  (left) and along  $\hat{x}$  (right), with the respective selection rules. (C) Time sequences of the applied MW fields (top) and the excitation schemes applied at each stage of the experiment (bottom).

In the ESST region (II), a sequence of three resonant, linearly polarized, and mutually orthogonally polarized MW fields is applied consecutively in the following order:  $|1_{01}\rangle \xleftarrow{\pi/2, \phi_a} |0_{00}\rangle \xrightarrow{\pi, \phi_c} |1_{10}\rangle \xrightarrow{\pi/2, \phi_b} |1_{01}\rangle$ , where  $\phi_i$  represents the phase of the MW field driving the  $i$ -type transition, with  $i = a, b$  or  $c$ . The enantiomer selectivity of ESST is determined by the relative phases of the MW fields. In the experiment, the phase of the final pulse  $\phi_b$  is scanned in  $20^\circ$  increments from  $0^\circ$  to  $720^\circ$ , while the phases of the first two MW fields,  $\phi_a$  and  $\phi_c$ , are kept fixed.

In the detection region (III), the same UV laser as used in the depletion region probes the population in the target rotational state, utilizing only about 10% of the laser power to avoid line broadening. The laser is aligned perpendicularly to the molecular beam and parallel to

the laser in the depletion region, thus interacting with the same group of molecules as in the depletion region. The laser-induced fluorescence (LIF) emitted by the molecules is detected using a photomultiplier tube (PMT).

In this experimental approach, the ESST signal, defined as the population in the target state  $|1_{01}\rangle$  at the end of the ESST process, is given by the following expression (29):

$$\frac{1}{2} [n_{0_{00}} + 4n_{1_{01}} + n_{1_{10}} \pm (n_{0_{00}} - n_{1_{01}}) \sin(\phi_a - \phi_c + \phi_b)] \quad (1)$$

where  $n_{0_{00}}$ ,  $n_{1_{01}}$ , and  $n_{1_{10}}$  is the initial population of each  $M_J$  sub-level of the states  $|0_{00}\rangle$ ,  $|1_{01}\rangle$ , and  $|1_{10}\rangle$ , respectively, at the beginning of the ESST process and where the  $\pm$  sign is used for different enantiomers. The amplitude-to-mean ratio of this expression is the measure for maximum state-specific enantiomeric enrichment, which refers to the enantiomeric excess achievable in a chosen rotational state when starting from a racemic mixture. Achieving 100% state-specific enantiomeric enrichment requires that both upper levels are initially empty, i.e.,  $n_{1_{01}} = n_{1_{10}} = 0$ . It is seen from this expression how any remaining population in states  $|1_{01}\rangle$  and  $|1_{10}\rangle$  adversely affects the state-specific enantiomeric enrichment. Moreover, population in the target state impacts the mean of the ESST signal four times more than population in state  $|1_{10}\rangle$ .

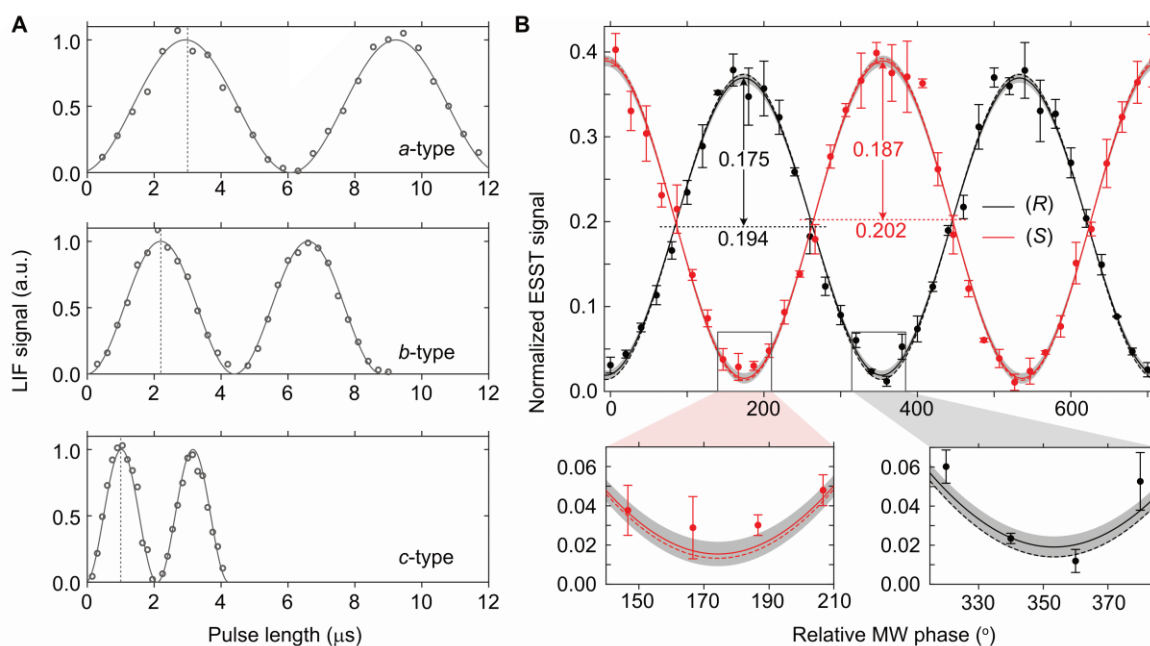


**Fig. 3. Rabi oscillation curves and ESST results.** (A) Rabi oscillation curves of the MW transitions are shown for (*R*)-1-indanol. The  $\pi$ -pulse durations are marked by dashed vertical lines. (B) Normalized ESST signal is shown as a function of the relative MW phase for (*R*)- and (*S*)-enantiomers in black and red, respectively. The standard error on each measurement point is indicated by error bars. Calculated normalized ESST curves using expression (1) are shown with dashed lines. The gray shaded areas around the experimental curves show the standard deviation from the sine fit. Two regions of specific interest are shown enlarged in the boxes below.

Measurements are performed using commercially available, enantiopure samples of 1-indanol. The enantiopurity for both samples is better than 99.8% as determined by chiral

high-performance liquid chromatography. Separate molecular beam sources are used for the two enantiomers to avoid any cross-contamination. To ensure an optimal  $\pi/2 - \pi - \pi/2$  pulse sequence, Rabi oscillation curves for each MW transition are measured prior to ESST. The  $\pi$ -pulse conditions are determined from the pulse durations that correspond to the first maxima of these curves, as indicated by vertical bars in Fig. 3A. Due to the use of different molecular beam sources, the  $\pi$ - pulse durations are slightly different for the measurements on the (*R*)- and (*S*)-enantiomer (see Supplementary Materials).

Figure 3B shows the ESST signals, normalized to the thermal population in the target state  $|1_{01}\rangle$ , as a function of the relative MW phase. The signals for the (*R*)- and (*S*)-enantiomers are shown in black and red, respectively, with error bars representing the standard errors. The mean and amplitude values from sinusoidal fits to the data are given. These values yield a maximum state-specific enantiomeric enrichment of 90.2(1.9)% for the (*R*)-enantiomer and 92.4(2.1)% for the (*S*)-enantiomer. The latter value corresponds to a state-specific enantiomeric purity of more than 96% when starting from a racemic mixture.

The two ESST curves in Fig. 3B are shown with a phase difference of exactly  $180^\circ$ . When using identical pulse durations for the (*R*)- and (*S*)-enantiomer, their ESST curves are indeed confirmed to be  $180^\circ$  out-of-phase (see Supplementary Materials). However, optimal transfer efficiency for both enantiomers is only obtained when using pulse durations that are optimized for each enantiomer individually. This results in an additional phase offset between the measurements, that has been corrected for in Fig. 3B.

In the experiments, approximately 2% of the original thermal populations in the states  $|1_{01}\rangle$  and  $|1_{10}\rangle$  is measured to be present in the detection region. This population is attributed to re-filling as a result of in-beam collisions with the carrier gas atoms while the molecules travel from the depletion region to the detection region (27, 29). This is confirmed by the observation that reducing the carrier gas density by installing a second skimmer is beneficial, i.e., that it reduces this population. When depleting just in front of the LIF detection region, basically no population is measured to be present. Using this information in a model as described in the Supplementary Materials, the population in both of these states is estimated to be about 1.4% upon entering the ESST region.

Calculated normalized ESST curves using expression (1) and assuming thermal populations at 1.1 K for (*R*)-indanol and 0.7 K for (*S*)-indanol, are shown in Figure 3B (dashed). These calculations incorporate the 1.4% population in the two upper levels as well as the 0.2% enantiomer-impurity. The calculated amplitude and mean of the normalized ESST signal agree very well with those of the experiment, for both enantiomers. The high degree of state-specific enantiomeric purity is best seen by the proximity of the minima of the sine curve to zero, and two relevant segments are therefore shown enlarged in Fig.3B.

The data presented here show full quantum state control of the chiral molecule 1-indanol to the extent that more than 96% enantiomer-selectivity can be obtained when starting from a racemic mixture. Currently, the only experimental limitation from reaching 100% enantiomer-selectivity stems from in-beam collisions, which can be avoided by reducing the distances between the three interaction regions. The experimental approach outlined here is universally applicable to the large majority of chiral molecules. With its capability to create enantiopure quantum states starting from a racemic mixture, this approach has the potential to significantly advance the experimental methods to measure parity-violation effects in chiral molecules (33). Moreover, by incorporating state-dependent deflection or focusing schemes (34), these measurements pave the way for spatial separation of chiral molecules in the gas phase.

## References

1. I. Weissbuch, M. Lahav, Crystalline Architectures as Templates of Relevance to the Origins of Homochirality. *Chemical Reviews* **111**, 3236-3267 (2011).
2. D. K. Kondepudi, R. J. Kaufman, N. Singh, Chiral Symmetry Breaking in Sodium Chlorate Crystallization. *Science* **250**, 975-976 (1990).
3. R. A. Rosenberg, M. Abu Haija, P. J. Ryan, Chiral-Selective Chemistry Induced by Spin-Polarized Secondary Electrons from a Magnetic Substrate. *Physical Review Letters* **101**, 178301 (2008).
4. Y. Yamagata, A hypothesis for the asymmetric appearance of biomolecules on earth. *Journal of Theoretical Biology* **11**, 495-498 (1966).
5. V. S. Letokhov, On difference of energy levels of left and right molecules due to weak interactions. *Physics Letters A* **53**, 275-276 (1975).
6. M. Quack, J. Stohner, M. Willeke, High-Resolution Spectroscopic Studies and Theory of Parity Violation in Chiral Molecules. *Annual Review of Physical Chemistry* **59**, 741-769 (2008).
7. B. Darquié, C. Stoeffler, A. Shelkovnikov, C. Daussy, A. Amy-Klein, C. Chardonnet, S. Zrig, L. Guy, J. Crassous, P. Soulard, P. Asselin, T. R. Huet, P. Schwerdtfeger, R. Bast, T. Saue, Progress toward the first observation of parity violation in chiral molecules by high-resolution laser spectroscopy. *Chirality* **22**, 870-884 (2010).
8. F. C. Muller, G. Muller, J. P. Riehl, Emission detected circular dichroism from long-lived excited states: Application to chiral Eu(III) systems. *Chirality* **19**, 826-832 (2007).
9. Y. He, B. Wang, R. K. Dukor, L. A. Nafie, Determination of Absolute Configuration of Chiral Molecules Using Vibrational Optical Activity: A Review. *Applied Spectroscopy* **65**, 699-723 (2011).
10. L. A. Nafie, T. A. Keiderling, P. J. Stephens, Vibrational circular dichroism. *Journal of the American Chemical Society* **98**, 2715-2723 (1976).
11. P. J. Stephens, Theory of vibrational circular dichroism. *The Journal of Physical Chemistry* **89**, 748-752 (1985).
12. D. Ayuso, A. F. Ordonez, O. Smirnova, Ultrafast chirality: the road to efficient chiral measurements. *Physical Chemistry Chemical Physics* **24**, 26962-26991 (2022).
13. M. Pitzer, M. Kunitski, A. S. Johnson, T. Jahnke, H. Sann, F. Sturm, L. P. H. Schmidt, H. Schmidt-Böcking, R. Dörner, J. Stohner, J. Kiedrowski, M. Reggelin, S. Marquardt, A. Schießler, R. Berger, M. S. Schöffler, Direct Determination of Absolute Molecular Stereochemistry in Gas Phase by Coulomb Explosion Imaging. *Science* **341**, 1096-1100 (2013).
14. I. Powis, Photoelectron Spectroscopy and Circular Dichroism in Chiral Biomolecules: L-Alanine. *The Journal of Physical Chemistry A* **104**, 878-882 (2000).
15. L. Nahon, G. A. Garcia, C. J. Harding, E. Mikajlo, I. Powis, Determination of chiral asymmetries in the valence photoionization of camphor enantiomers by photoelectron imaging using tunable circularly polarized light. *The Journal of Chemical Physics* **125**, 114309 (2006).
16. D. Patterson, M. Schnell, J. M. Doyle, Enantiomer-specific detection of chiral molecules via microwave spectroscopy. *Nature* **497**, 475 (2013).
17. D. Patterson, J. M. Doyle, Sensitive Chiral Analysis via Microwave Three-Wave Mixing. *Physical Review Letters* **111**, 023008 (2013).
18. S. Eibenberger, J. Doyle, D. Patterson, Enantiomer-Specific State Transfer of Chiral Molecules. *Physical Review Letters* **118**, 123002 (2017).
19. C. Pérez, A. L. Steber, S. R. Domingos, A. Krin, D. Schmitz, M. Schnell, Coherent Enantiomer-Selective Population Enrichment Using Tailored Microwave Fields. *Angewandte Chemie International Edition* **56**, 12512-12517 (2017).

20. P. Král, M. Shapiro, Cyclic Population Transfer in Quantum Systems with Broken Symmetry. *Physical Review Letters* **87**, 183002 (2001).
21. Y. Fujimura, L. González, K. Hoki, D. Kröner, J. Manz, Y. Ohtsuki, From a Racemate to a Pure Enantiomer by Laser Pulses: Quantum Model Simulations for H<sub>2</sub>POSH. *Angewandte Chemie International Edition* **39**, 4586-4588 (2000).
22. E. Hirota, Triple resonance for a three-level system of a chiral molecule. *Proceedings of the Japan Academy, Series B* **88**, 120-128 (2012).
23. S. Lobsiger, C. Perez, L. Evangelisti, K. K. Lehmann, B. H. Pate, Molecular Structure and Chirality Detection by Fourier Transform Microwave Spectroscopy. *The Journal of Physical Chemistry Letters* **6**, 196-200 (2015).
24. K. K. Lehmann, Influence of spatial degeneracy on rotational spectroscopy: Three-wave mixing and enantiomeric state separation of chiral molecules. *The Journal of Chemical Physics* **149**, 094201 (2018).
25. Q. Zhang, Y.-Y. Chen, C. Ye, Y. Li, Evading thermal population influence on enantiomeric-specific state transfer based on a cyclic three-level system via ro-vibrational transitions. *Journal of Physics B: Atomic, Molecular and Optical Physics* **53**, 235103 (2020).
26. M. Leibscher, J. Kalveram, C. P. Koch, Rational Pulse Design for Enantiomer-Selective Microwave Three-Wave Mixing. *Symmetry* **14**, (2022).
27. J. Lee, J. Bischoff, A. O. Hernandez-Castillo, B. Sartakov, G. Meijer, S. Eibenberger-Arias, Quantitative study of enantiomer-specific state transfer. *Physical Review Letters* **128**, 173001 (2022).
28. H. Singh, F. E. L. Berggötz, W. Sun, M. Schnell, Chiral Control of Gas-Phase Molecules using Microwave Pulses. *Angewandte Chemie International Edition* **62**, e202219045 (2023).
29. J. H. Lee, J. Bischoff, A. O. Hernandez-Castillo, E. Abdiha, B. G. Sartakov, G. Meijer, S. Eibenberger-Arias, The influence of microwave pulse conditions on enantiomer-specific state transfer. *arXiv:2310.11120*, (2023).
30. C. Ye, Q. Zhang, Y. Li, Real single-loop cyclic three-level configuration of chiral molecules. *Physical Review A* **98**, 063401 (2018).
31. A. O. Hernandez-Castillo, J. Bischoff, J. H. Lee, J. Langenhan, M. Karra, G. Meijer, S. Eibenberger-Arias, High-resolution UV spectroscopy of 1-indanol. *Physical Chemistry Chemical Physics* **23**, 7048-7056 (2021).
32. K. Le Barbu-Debus, F. Lahmani, A. Zehnacker-Rentien, N. Guchhait, S. S. Panja, T. Chakraborty, Fluorescence spectroscopy of jet-cooled chiral ( $\pm$ )-indan-1-ol and its cluster with ( $\pm$ )-methyl- and ethyl-lactate. *The Journal of Chemical Physics* **125**, (2006).
33. I. Erez, E. R. Wallach, Y. Shagam, Simultaneous Enantiomer-Resolved Ramsey Spectroscopy Scheme for Chiral Molecules. *Physical Review X* **13**, 041025 (2023).
34. S. Y. T. van de Meerakker, H. L. Bethlem, N. Vanhaecke, G. Meijer, Manipulation and Control of Molecular Beams. *Chemical Reviews* **112**, 4828-4878 (2012).

**Acknowledgments:** We are grateful to Johannes Bischoff and Alicia Hernandez-Castillo for their contributions to earlier stages of the experiment. We thank Marco De Pas, Sebastian Kray, Henrik Haak, Daniel Fontoura Barroso and Russell Thomas as well as the teams of the mechanical and electronics workshop of the Fritz Haber Institute for excellent technical and laser support. We acknowledge funding by the European Union (ERC, COCOCIMO, 101116866).